J Mater Sci (2011) 46:4071–4078
DOI 10.1007/s10853-011-5336-8

Use of L-tyrosine amino acid as biomodifier of Cloisite Na^+ for preparation of novel poly(vinyl alcohol)/organoclay bionanocomposites film

Shadpour Mallakpour · Maryam Madani

Received: 8 September 2010 / Accepted: 27 January 2011 / Published online: 10 February 2011

Abstract Cloisite Na^+ was modified via cation exchange reaction using natural L-tyrosine amino acid. This novel chiral organo-modified Cloisite Na^+ was characterized using fourier transform infrared spectroscopy (FT–IR), X-ray diffraction (XRD), and thermogravimetric analysis/derivative thermal gravimetric (TGA/DTG). Then, polymer bionanocomposites were prepared by dispersing chiral organo-modified Cloisite Na^+ in poly(vinyl alcohol) (PVA) via ultrasonic irradiation. The novel bionanocomposites were characterized by FT–IR, UV–Visible, TGA, and XRD. Scanning electron microscopy and transmission electron microscopy were used to obtain the information about morphological structure of PVA/Cloisite Na^+/Tyr bionanocomposites. The results showed that a mixture of intercalated and exfoliated Cloisite Na^+ dispersion in PVA matrix. The TGA data was compared with the pure PVA and the results showed that the introduction of a small amount of Cloisite Na^+/Tyr led to improvement in thermal stability of the obtained new bionanocomposites. UV–Visible transmission spectra of pure PVA and new bionanocomposites film in the visible light region (400–800 nm) showed that they are rather transparent.

S. Mallakpour (✉) · M. Madani
Department of Chemistry, Organic Polymer Chemistry Research Laboratory, Isfahan University of Technology, 84156-83111 Isfahan, Islamic Republic of Iran
e-mail: mallak@cc.iut.ac.ir

S. Mallakpour
Nanotechnology and Advanced Materials Institute, Isfahan University of Technology, 84156-83111 Isfahan, Islamic Republic of Iran

Introduction

Recently, polymer nanocomposites are the subject of increased interest because of the unique properties that can be achieved with these materials. Owing to the nanoscale dispersion of the inorganic phase, very small filler content is enough to affect several properties of polymer matrix; thereby, their physical, thermal, and mechanical properties could be improved [1–5]. One of the nanofiller materials is nanolayer of montmorillonite (MMT). Nanocomposites consisting of these materials and organic polymers have suggested extreme investigation interests in recent times because their unique characteristics produce many potentially commercial applications. They can be transformed into novel materials possessing the advantages of both organic materials, such as light weight, flexibility, and good moldability, and inorganic materials, such as high strength, heat stability, and chemical resistance. Materials incorporating polymer/MMT hybrids can be able to achieve advanced degrees of stiffness, strength, and gas-barrier properties with the addition of small amount of inorganic substance [6–8].

MMT has medicinal properties and have been used for drug delivery and drug release systems [9–11]. It is composed of units made of two silica tetrahedral sheets centered with an alumina octahedral sheet, which is called 2:1 phyllosilicate that is able to forming stable suspensions in water. Its layers are stacked by weak dipolar or van der Waals forces, and it has both surface and edge charges. The charges on edges are simply available to modification [12–15]. To insure good compatibility between polymer and MMT in the preparation of nanocomposites, modification of the MMT is necessary. This modification causes an increase in the *d*-spacing, which facilitates the entry of the polymer into the clay gallery. This is usually done by

cationic exchange using alkylammonium salts [16–20]. Amino acids possess the potential to be used as modifiers, which can increase the interlayer spacing of clay and improve its biodegradability [21, 22].

Poly(vinyl alcohol) (PVA) is highly biocompatible, non-toxic, and a water-soluble polymer [23–25]. This polymer has many applications in textile industry, membrane manufacturing, medical, cosmetic, food, packaging industries, and paper coating, because of its high tensile, impact and abrasion resistance, high biocompatibility and high barrier properties [26–29]. Owing to wide range applications of PVA, many efforts have been done to improve the properties of this polymer. The performances of PVA nanocomposite films depend on the properties of nanofillers, preparation methods, and the final nanostructures. Nanoclays such as MMT, is shown to have a significant effect on the properties of PVA nanocomposites which are attributed to the strong interactions between the nanoparticle and polymer matrix [30]. PVA/clay nanocomposites have been studied in many laboratories [31–33]. Sammon and co-workers [33] prepared PVA/MMT nanocomposites using solution intercalation method and performed in situ diffusion experiments of water and acetone into nanocomposites. Strawhecker and Manias [12] prepared the PVA/clay nanocomposites by casting the water suspension of PVA and MMT. Room temperature distilled water was used to form a suspension of Na^+-MMT. The TEM photograph of 20 wt% clay containing nanocomposite reveals the co-existence of silicate layers in the intercalated and exfoliated states.

In this investigation, at first, protonated form of L-tyrosine amino acid (Tyr) was used as biomodifier for modification of Cloisite Na^+, which can increase the interlayer spacing of Cloisite Na^+ and also improve its biodegradability. Intercalation of amino acid between nanolayer of Cloisite Na^+ was studied by different techniques. Then, PVA/Cloisite Na^+/Tyr bionanocomposites (BNCs) with different compositions were fabricated using ultrasonic irradiation. Furthermore, the films of these BNCs were prepared via solution casting method and were fully characterized by different methods.

Experimental

Materials

PVA $-[(CH_2CHOH)]_n-$ used in this study was purchased from Merck Chemical Co., Mw = 145,000 g/mol with a degree of hydrolysis of 98%. L-Tyrosine ($C_9H_{11}O_3N$, Mw = 181.19 g/mol) and hydrochloric acid (HCl, 37%) were purchased from Merck Chemical Co. Cloisite Na^+ was obtained from southern clay products, Gonzales, Texas (USA) with a cation exchange capacity (CEC) of 92.6 mequiv/100 g of Cloisite Na^+.

Preparation of the chiral organo-modified Cloisite Na^+

Ion exchange method was used to prepare organo-modified Cloisite Na^+. At first Tyr was placed in a beaker, followed by the addition of concentrated hydrochloric acid and 50 mL of deionized water. This solution was heated at 80 °C for 3 h. In another beaker, Cloisite Na^+ was dispersed in 150 mL of deionized water for 3 h. The both solutions were mixed, and the resulting mixture vigorously was stirred at 60 °C for 6 h. The solution containing the organo-modified Cloisite Na^+ was filtered warmly and washed with hot deionized water to remove chloride anions. The organically modified Cloisite Na^+ was dried at 60 °C for 6 h. The dried precipitates was ground and screened with a 325-mesh sieve.

Preparation of PVA/Cloisite Na^+/Tyr BNCs film

PVA/Cloisite Na^+/Tyr BNCs film with different Cloisite Na^+/Tyr content (5, 10, and 15%) were fabricated by using the solution casting method. In a typical procedure, for each composition, 1 g of PVA was dissolved in 20 mL of deionized water at 90 °C under continuous stirring for at least 30 min. Organo-modified Cloisite Na^+ solutions (>1 wt%) were obtained by suspending a measured amount of Cloisite Na^+/Tyr (5, 10, and 15% vs. PVA, respectively) in deionized water at 40 °C under stirring for 3 h and sonicated for 30 min (using a MISONIX ultrasonic liquid processor, XL-2000 SERIES. Ultrasound was a wave of frequency 2.25×10^4 Hz and power of 100 W). Both solutions are mixed, stirred for 6 h at 90 °C, and again sonicated for 30 min. The mixture was poured into a Petri dish. These films were dried at 40 °C for 24 h.

Characterizations

Infrared spectroscopy (FT–IR)

Spectra of Cloisite Na^+, Cloisite Na^+/Tyr, and Tyr samples were recorded from KBr pellets. Spectra of the blend films of PVA/Cloisite Na^+/Tyr were recorded with a Jasco-680 FT–IR spectrophotometer (Japan) in transmittance mode from 400 to 4000 cm^{-1} with resolution of 4 cm^{-1}.

X-ray diffraction (XRD)

The XRD measurements were performed for the Cloisite Na^+, organo-modified Cloisite Na^+, and the BNC films using a Bruker, D8ADVANCE (Germany). Ni-filtered CuKa radiation utilized at 45 kV and 100 mA. Wavelength

of emitted radiation is 1.54056 Å. The samples were scanned in the 2θ mode using a step scanning method with a step-width of 0.02°/min in the range from $2\theta = 1.4^\circ$ to 10°.

Thermal gravimetric analysis (TGA)

The TGA of Cloisite Na^+, Cloisite Na^+/Tyr, pure PVA and BNC films were carried out on STA503 Win TA instrument at a heating rate of 10 °C/min under flowing nitrogen from room temperature to 800 °C. All samples were dried under vacuum for 4 h at 60 °C prior to be tested.

UV–Visible spectroscopy

The UV–Visible transmission spectra of BNC films were measured using JASCO V-750 UV–Visible spectrometer in the spectra range from 200 to 800 nm.

Scanning electron microscopy (SEM)

The morphology of PVA/Cloisite Na^+/Tyr BNC film was observed by means of scanning electron microscope (XL30, Philips) at an accelerating voltage of 5 kV.

Transmission electron microscopy (TEM)

TEM micrograph of PVA/Cloisite Na^+/Tyr BNC was obtained with a Philips CM 120 model at an accelerating voltage of 100 kV.

Results and discussion

Preparation and characterization of organoclay

Chiral organo-modified Cloisite Na^+ was prepared by replacing Na^+ cation in this nanoclay with protonated form of Tyr. This modification increased organophilicity of Cloisite Na^+, therefore dispersion of this nanoclay in polymer matrix was improved (scheme 1). The chemical structure, diffraction pattern, and thermal behavior of this organoclay were verified by FT–IR, XRD, and TGA/DTG.

The FT–IR spectra of Tyr, Cloisite Na^+, and Cloisite Na^+/Tyr are shown in Fig. 1. The spectrum of Cloisite Na^+ shows the characteristic bands 3626 cm^{-1} due to O–H stretching (sharp peak) for Al–OH and Si–OH, a broad peak centered on 3441 cm^{-1} due to interlayer and H-bonded –OH, 1637 cm^{-1} is attributed to –OH bending mode in water, 1044 cm^{-1} due to Si–O stretching, 918 and 798 cm^{-1} due to AlAlOH and AlMgOH bending vibrations and 525 and 468 cm^{-1} due to the Si–O–Al and Si–O–Si bending vibrations. In the spectrum of Tyr, broad peak which was

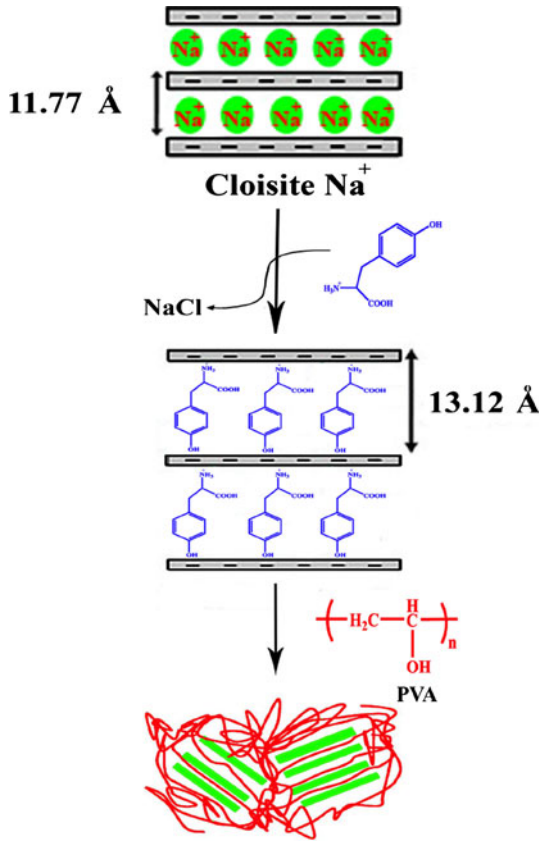

Scheme 1 Schematic representation of the modification of Cloisite Na^+ with L-Tyr and its subsequent use to produce BNCs

observed between 3203 and 3125 cm^{-1} corresponds to N–H and acidic O–H stretching, at 2960 and 2752 cm^{-1} which correspond to C–H stretching of alkyl chain. The peaks which were observed at 1609, 1590, 1521, and 1416 cm^{-1} could be attributed to N–H asymmetric bending vibration, C=O asymmetric stretching, N–H symmetric bending vibration and C=O symmetric stretching, respectively. Cloisite Na^+/Tyr spectrum shows small broad peak between 3300 and 2700 cm^{-1} compare with the spectrum of pure Cloisite Na^+ which could be attributed to acidic OH of Tyr. On the other hand, N–H bending and C=O stretching related to Tyr which were observed at 1577 and 1517 cm^{-1} showed small shift due to hydrogen bonding of protonated form of Tyr with Cloisite Na^+. All of this data revealed the presence of Tyr moieties in the Cloisite Na^+/Tyr system.

The XRD patterns of Cloisite Na^+, Cloisite Na^+/Tyr are shown in Fig. 2. The peak corresponding to pristine Cloisite Na^+ is observed at $2\theta = 7.5^\circ$. The *d*-spacing at this value of 2θ is 11.77 Å. In the case of Cloisite Na^+ modified with Tyr, the peak appears at $2\theta = 6.6^\circ$, which related to a *d*-spacing of 13.12 Å. The interlayer spacing of Cloisite Na^+ was obviously increased after the treatment with Tyr. The result suggested that this novel biomodifier successfully

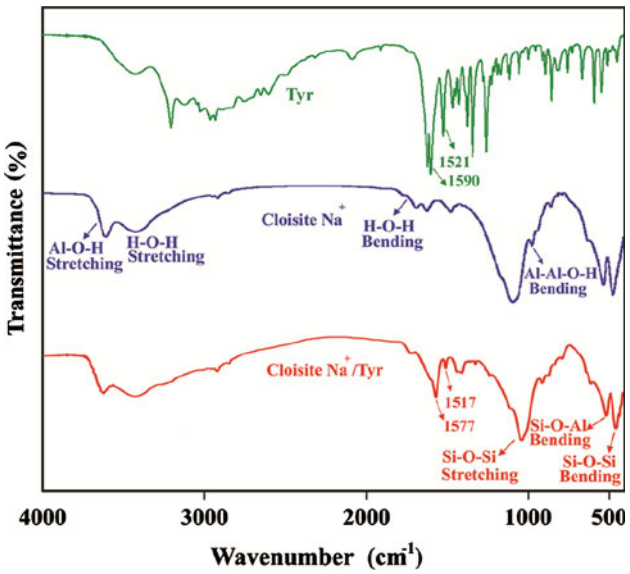

Fig. 1 FT–IR spectra of Tyr, Cloisite Na^+, and Cloisite Na^+/Tyr

intercalated between layers of Cloisite Na^+. The results of the XRD patterns are summarized in Table 1.

The TGA/DTG curves for Cloisite Na^+ and organo-modified Cloisite Na^+ are shown in Fig. 3a, c. Decomposition of Cloisite Na^+ occurs in two steps: desorption of water from the interlayer space happened around 100–200 °C which is about 1% weight loss and dehydroxylation of the layer crystal lattice structure took place around 700 °C Cloisite Na^+ [34]. The thermal degradation of Cloisite Na^+/Tyr show three weight loss stages: the first weight loss occurs around 100 °C due to water trapped in the Cloisite Na^+/Tyr chiral organoclay. The second step corresponds to decomposition of the organic parts present in the Cloisite Na^+/Tyr system with a maximum

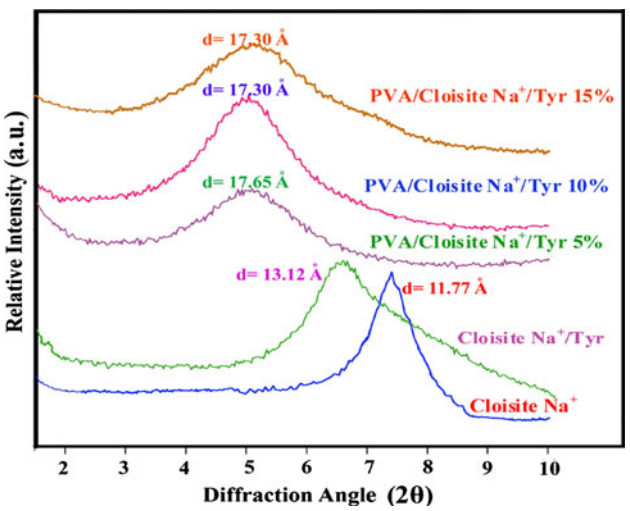

Fig. 2 XRD patterns of Cloisite Na^+, Cloisite Na^+/Tyr, and different PVA/Cloisite Na^+/Tyr BNCs

Table 1 *d*-Value of Cloisite Na^+, modified Cloisite Na^+ and PVA/Cloisite Na^+/Tyr BNCs with different Cloisite Na^+/Tyr contents

Sample	2θ (degree)	d (Å)
Cloisite Na^+	7.5	11.77
Cloisite Na^+/Tyr	6.6	13.12
PVA/Cloisite Na^+/Tyr 5%	5.0	17.65
PVA/Cloisite Na^+/Tyr10%	5.1	17.30
PVA/Cloisite Na^+/Tyr 15%	5.1	17.30

decomposition around 290–300 °C and third decomposition occurred around 600 °C.

Preparation and characterization of PVA/Cloisite Na^+/Tyr bionanocomposite films

PVA/Cloisite Na^+/Tyr BNCs with different compositions were fabricated using ultrasonic irradiation. Furthermore, the films of these BNCs were prepared via solution casting method. The schematic preparation of BNC is shown in scheme 1. The BNCs were characterized by FT–IR, XRD, SEM, TEM, TGA, and UV–Visible, respectively.

FT–IR spectra pure PVA and PVA/Cloisite Na^+/Tyr BNCs (5, 10, and 15% of Cloisite Na^+/Tyr) are shown in Fig. 4. The frequencies and assignments for the pure PVA (Fig. 4b) are indicated as follows: very intensive, broad hydroxyl band occurs at 3000–3400 cm^{-1}, bands at 2941 cm^{-1} are due to stretching vibrations of –CH and CH_2 groups, resulting of residual acetate groups, is depicted at 1713 cm^{-1} in PVA spectrum. A band attributed to C–O stretching is presented at 1093 cm^{-1}. All these bands are also observed in BNCs film with Cloisite Na^+/Tyr (Fig. 4c–e) which indicates the dispersion of chiral organoclay into PVA matrix. The very small shifts of absorption maximum are due to changes in the nearest surrounding of functional groups. As the loading of Cloisite Na^+/Tyr is increased, the intensities of organoclay bands become stronger in the FT–IR spectra of the obtained BNC films.

Figure 2 shows the diffraction patterns of PVA/Cloisite Na^+/Tyr BNCs with 5, 10, and 15% contents. PVA/Cloisite Na^+/Tyr BNC 5% showed a peak at $2\theta = 5.0^\circ$ ($d = 17.65$ Å), for 10 and 15%, the peaks appeared at $2\theta = 5.1^\circ$ ($d = 17.30$ Å). In the BNCs film, these peaks are almost at the same position, indicating interlayer spacing increased in compared to Cloisite Na^+/Tyr organoclay. This is evidence that these Cloisite Na^+/Tyr are intercalated in PVA matrix, because for intercalated nanocomposites, the finite layer expansion associated with the polymer intercalation results in the appearance of a new basal reflection corresponding to the larger gallery height. On the other hand, for exfoliated structure, no more diffraction peaks are visible in the XRD diffractograms either because of a much too large spacing

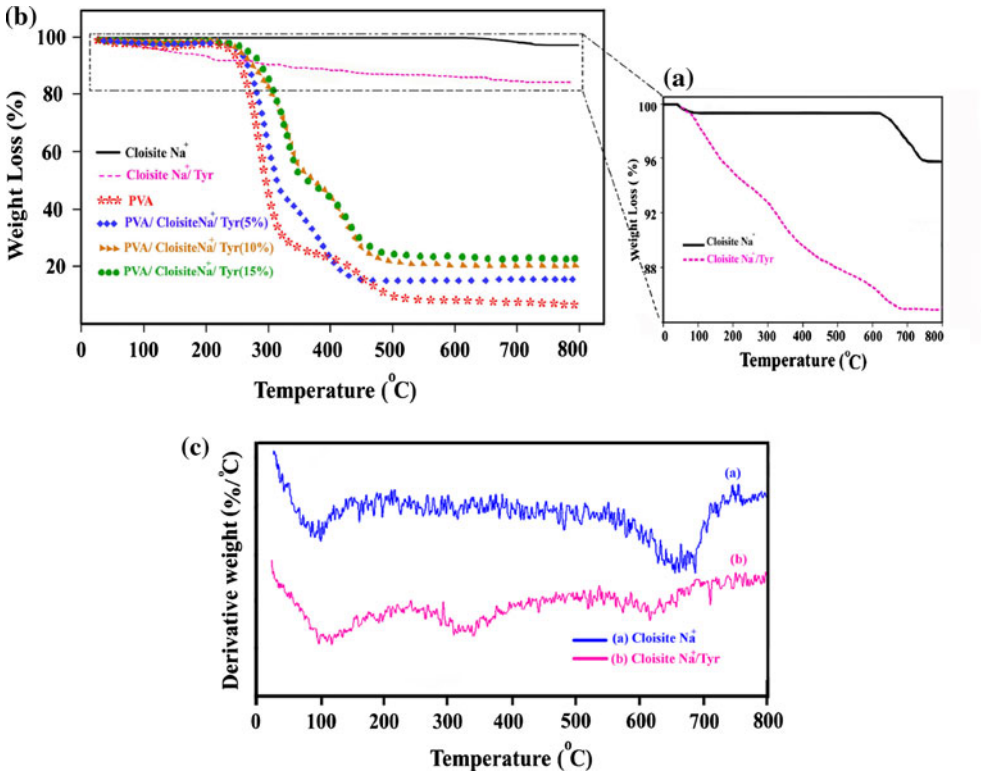

Fig. 3 TGA thermograms of **a** Cloisite Na^+, Cloisite Na^+/Tyr, **b** pure PVA and PVA/Cloisite Na^+/Tyr BNC with different Cloisite Na^+/Tyr contents **c** DTG of Cloisite Na^+, Cloisite Na^+/Tyr

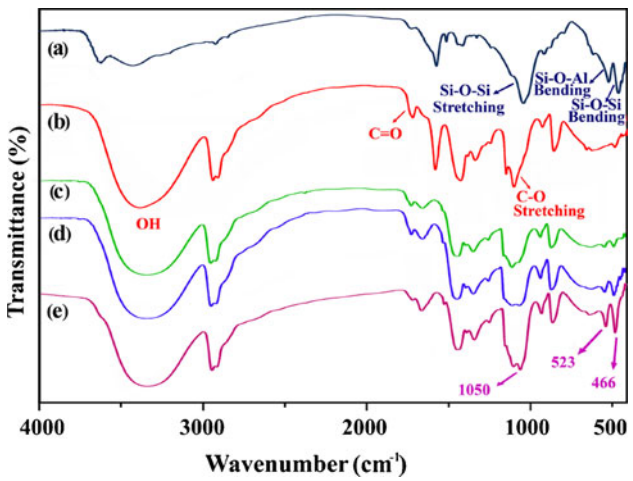

Fig. 4 FT–IR spectra of **a** Cloisite Na^+/Tyr, **b** pure PVA and PVA/Cloisite Na^+/Tyr BNCs with different Cloisite Na^+/Tyr contents **c** 5%, **d** 10%, and **e** 15%

between the layers or because the nanocomposite dose not present ordering anymore [1].

Morphology

The morphological micrograph of the BNC was studied by SEM, as shown in Fig. 5. The micrograph of PVA/Cloisite Na^+/Tyr BNC film with 10% of organoclay is well and regularly dispersed in the PVA matrix. The white strands in the SEM images correspond to Cloisite Na^+/Tyr platelets.

TEM images can give information about the morphology of BNCs. Typical TEM micrographs of the PVA/Cloisite Na^+/Tyr BNC film with 10% of organoclay is illustrated in Fig. 6, which the dark lines are the layers of Cloisite Na^+/Tyr. This TEM photograph demonstrates that most of Cloisite Na^+/Tyr were intercalated and less exfoliated dispersed homogeneously into the PVA matrix. The clay layers were also shown to be well dispersed in the PVA hybrids by the XRD profiles, as discussed previously.

Thermal stability of PVA/Cloisite Na^+/Tyr BNCs film with different Cloisite Na^+/Tyr contents

All samples were dried in vacuum before TGA test. The TGA measurements of pure PVA and Cloisite Na^+/Tyr BNCs with different Cloisite Na^+/Tyr contents are shown in Fig. 3b. The thermal decomposition behavior of pure PVA and PVA/Cloisite Na^+/Tyr BNCs with different percent of Cloisite Na^+/Tyr passes through three steps when heated from 25 to 800 °C. In the first step, up to 200 °C, there is nearly no difference between the pure PVA and the PVA/Cloisite Na^+/Tyr BNCs in thermal stability. The second decomposition temperatures of pure PVA, due to the elimination of side-groups at lower temperature, occurred at 200–325 °C and finally the third step around 600 °C due to the decomposition of main chain of PVA [35]. The pure PVA displays the lowest thermal stability

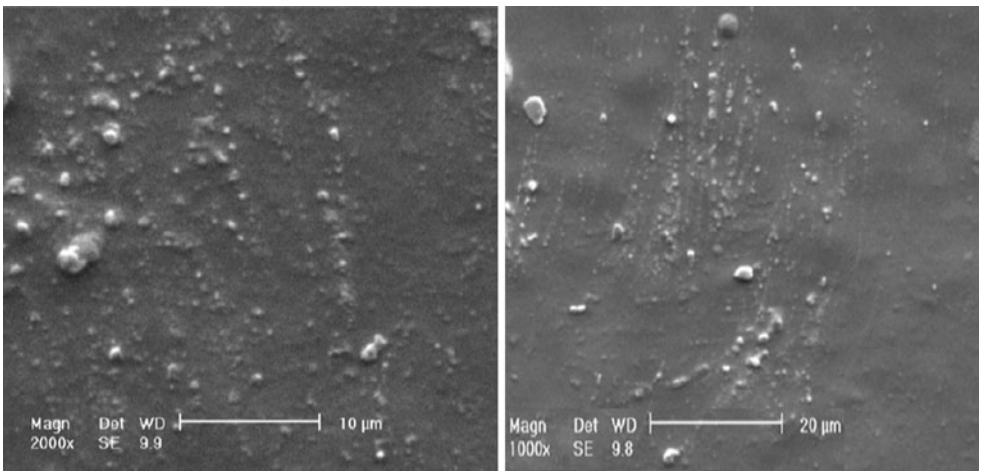

Fig. 5 SEM micrograph of PVA/Cloisite Na^+/Tyr (10%)

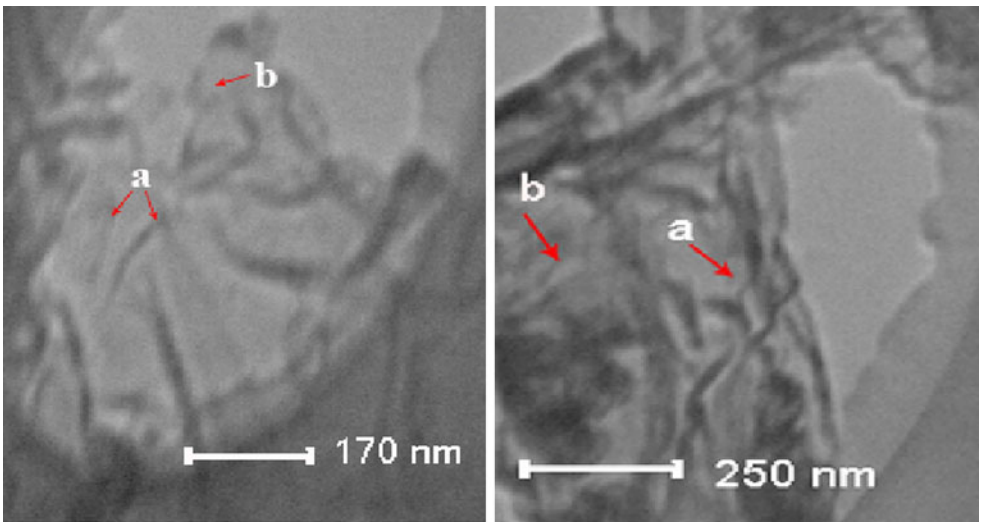

Fig. 6 TEM micrograph of PVA/Cloisite Na^+/Tyr (10%), **a** intercalated and **b** exfoliated

and major weight losses are observed in the range of, 200–500 °C for BNC films. The thermal stability of the BNCs film was increased with Cloisite Na^+/Tyr content. The improvement of thermal stability can be explained through the reduced mobility of the PVA chains in the obtained BNCs. Because of reduced chain mobility, the chain transfer reaction will be suppressed and, consequently, the degradation process will be slowed and decomposition will take place at higher temperatures [36]. The temperature of 5 and 10% weight loss together with char yield at 700 °C for Cloisite Na^+, modified Cloisite Na^+, and PVA/Cloisite Na^+/Tyr BNC with different Cloisite Na^+/Tyr contents have been calculated from their thermograms. The thermal analysis data are summarized in Table 2. The char yield at 700 °C of the BNCs with different Cloisite Na^+/Tyr content is higher than that of pure

Table 2 Weight loss (%) at different heating temperatures for the thermal decomposition of pure PVA and PVA/Cloisite Na^+/Tyr BNCs with different Cloisite Na^+/Tyr contents

PVA BNCs	Weight loss (%)		
	T_5[a] (°C)	T_{10}[b] (°C)	Char yield[c] (%)
Pure PVA	237	254	7.9
PVA/Cloisite Na^+/Tyr (5%)	248	264	14.64
PVA/Cloisite Na^+/Tyr (10%)	255	280	18.61
PVA/Cloisite Na^+/Tyr (15%)	263	300	21.12

[a] Temperature at which 5% weight loss was recorded by TGA at heating rate of 10 °C min^{-1} in N_2

[b] Temperature at which 10% weight loss was recorded by TGA at heating rate of 10 °C min^{-1} in N_2

[c] Percentage weight of material left undecomposed after TGA analysis at maximum temperature 700 °C in N_2

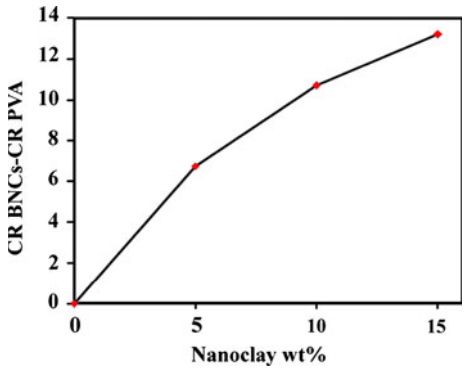

Fig. 7 Char yield of nanocomposite—char yield PVA as a function of nanoclay wt%

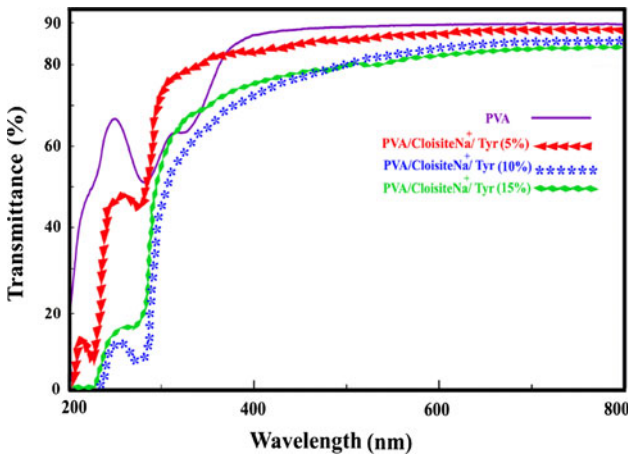

Fig. 8 UV-Visible transmittance spectra of PVA and PVA/Cloisite Na^+/Tyr BNCs film containing 5, 10, and 15% Cloisite Na^+/Tyr

PVA. This enhancement of the char formation is ascribed to the high heat resistance exerted by the Cloisite Na^+/Tyr. The influence of Cloisite Na^+/Tyr loading on the char formation of BNC films is shown in Fig. 7. Upon increasing the amount of Cloisite Na^+/Tyr char yields of BNCs are enhanced.

Optical transparency

Figure 8 shows UV–Visible transmission spectra of PVA and BNC films by different Cloisite Na^+/Tyr content. In the visible light region (400–800 nm) the PVA shows about 90% transparency, but transparency of BNC films with increasing the amount of Cloisite Na^+/Tyr were decreased. Owing to light scattering of clay nanolayer, UV regions (200–400 nm), are affected by the presence of the bionanoclay loading in the BNCs films. This can be explained by that Cloisite Na^+/Tyr dispersed uniformly in nanoscale in the PVA matrix. Figure 9 also exhibits the optical transparency of PVA and BNCs film with different bionanoclay content. For this purpose the samples of BNCs film have been placed above a pattern and the photographs have been taken. The levels of transparency of these films are similar to that of pure PVA film and slightly affected by increasing the amount of organoclay loading.

Conclusions

Amino acids possess the potential to be used as modifiers, which can increase the interlayer spacing of clay and improve its biodegradability. Therefore, in this investigating chiral L-Tyr was used for the modification of Cloisite Na^+. The intercalation of the Cloisite Na^+ was confirmed by XRD pattern. Then PVA/Cloisite Na^+/Tyr BNC films were prepared by effectively dispersing of the inorganic nanolayers in PVA matrix by ultrasonic irradiation. BNCs of PVA are characterized by FT–IR spectroscopy, XRD, TGA, and TEM. Morphological images of PVA/Cloisite Na^+/Tyr is studied through SEM. Thermal stability and optical clarity of PVA as well as PVA/Cloisite Na^+/Tyr is also investigated by TGA and UV–Visible transmission spectra, respectively. The incorporation of nanolayers of modified Cloisite Na^+ in PVA matrix resulted in an increase in thermal decomposition temperature based on TGA. Furthermore, from UV–Visible data, although transparency of the obtained BNCs film was decreased

Fig. 9 Transparency of PVA and BNCs film

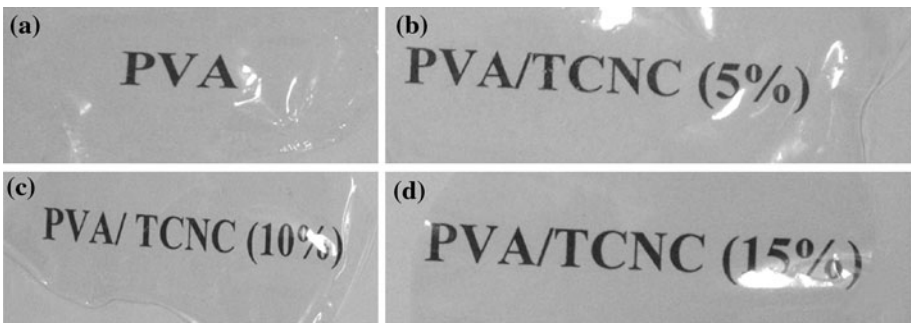

upon increasing the amount of nanoclay, but it could be concluded that they still show comparable transparency to the pure PVA film.

Acknowledgement The authors wish to express the gratitude to the Research Affairs Division Isfahan University of Technology (IUT), Isfahan, for partial financial support. Further financial support from National Elite Foundation (NEF) and Center of Excellency in Sensors and Green Chemistry Research (IUT) is gratefully acknowledged. Useful help from M. Dinari and A.V. Barati is also gratefully acknowledged.

References

1. Alexandre M, Dubois P (2000) Mater Sci Eng 28:1
2. Ray SS, Okamoto M (2003) Prog Polym Sci 28:1539
3. Tyan HL, Liu YC, Wei KH (1999) Chem Mater 11:1942
4. Tian H, Tagaya H (2008) J Mater Sci 43:766. doi:10.1007/s10853-007-2127-3
5. Mohan TP, Ramesh Kumar M, Velmurugan R (2006) J Mater Sci 41:2929. doi:10.1007/s10853-006-5164-4
6. Liu L, Qi Z, Zhu X (1999) J Appl Polym Sci 71:1133
7. Kar S, Maji PK, Bhowmick AK (2010) J Mater Sci 45:64. doi:10.1007/s10853-009-3891-z
8. Zunjarra SC, Sriraman R, Singh RP (2006) J Mater Sci 41:2219. doi:10.1007/s10853-006-7179-2
9. Takahashi T, Yamada Y, Kataoka K, Nagasaki Y (2005) J Controlled Release 107:408
10. Viseras C, Aguzzi C, Cerezo P, Lopez-Galindo A (2007) Appl Clay Sci 36:37
11. Rieux AD, Fievez V, Garinot M, Schneider YJ, Preat V (2006) J Controlled Release 116:1
12. Strawhecker KE, Manias E (2000) Chem Mater 12:2943
13. Utracki LA, Sepehr M, Boccaleri E (2007) Polym Adv Technol 18:1
14. Itoh T, Ohta N, Shichi T, Yui T, Takagi K (2003) Langmuir 19:9120
15. Greenwell HC, Jones W, Coveney PV, Stackhouse S (2006) J Mater Chem 16:708
16. Kornmann X, Lindberg H, Berglund LA (2001) Polymer 42:4493
17. Lee SY, Cho WJ, Kim KJ, Ahn JH, Lee M (2005) J Colloid Interface Sci 284:667
18. Tiwari RR, Khilar KC, Natarajan U (2008) Appl Clay Sci 38:203
19. Zhu J, He H, Zhu L, Wen X, Deng F (2005) J Colloid Interface Sci 286:239
20. Edwards G, Halley P, Kerven G, Martin D (2005) Thermochim Acta 429:13
21. Katti KS, Ambre AH, Peterka N, Katti DR (2010) Phil Trans R Soc A 368:1963
22. Katti DR, Ghosh P, Schmidt S, Katti KS (2005) Biomacromolecules 6:3276
23. Ren G, Xu X, Liu Q, Cheng J, Yuan X, Wu L, Wan Y (2006) React Funct Polym 66:1559
24. Shao C, Kim HY, Gong J, Ding B, Lee DR, Park SJ (2003) Mater Lett 57:1579
25. Krumova M, Lopez D, Benavente R, Mijangos C, Perena JM (2000) Polymer 41:9265
26. Chrissafis K, Paraskevopoulos KM, Papageorgiou G, Bikiaris DN (2008) J Appl Polym Sci 110:1739
27. Hassan CM, Peppas NA (2000) Adv Polym Sci 153:37
28. Yeum JH, Kwak JW, Han SS, Kim SS, Ji BC, Noh SK, Lyoo WS (2004) J Appl Polym Sci 94:1435
29. Stammen JA, Williams S, Ku DN, Guldberg RE (2001) Biomaterials 22:799
30. Yeh JT, Xu P, Tsai FC (2007) J Mater Sci 42:6590. doi:10.1007/s10853-007-1500-6
31. Nakane K, Yamashita T, Iwakura K, Suzuki F (1999) J Appl Polym Sci 74:133
32. Chang JH, Jang TG, Ihn KJ, Lee WK, Sur GS (2003) J Appl Polym Sci 90:3208
33. Doppers LM, Breen C, Sammon C (2004) Vib Spectrosc 35:27
34. Xiea W, Gaoa Z, Liua K, Pana WP, Vaiab R, Doug H, Singhd A (2001) Thermochim Acta 367–368:339
35. Alkan M, Benlikaya R (2009) J Appl Polym Sci 112:3764
36. Kuljanin J, Comor MI, Djokovic V, Nedeljkovic JM (2006) Mater Chem Phys 95:67